Volumetric Quasi-conformal Mappings
Quasi-conformal Mappings for Volume Deformation with Applications to Geometric Modeling

Alexander Naitsat[1], Emil Saucan[1,2] and Yehoshua Y. Zeevi[3]

[1]*Department of Mathematics, Technion, Haifa, Israel*
[2]*School of Mathematical Sciences, Dalian University of Technology, Dalian, China*
[3]*Electrical Engineering Department, Technion, Haifa, Israel*
{*anaitsat,semil*}*@tx.technion.ac.il, zeevi@ee.technion.ac.il*

Abstract: Due to intrinsic differences between surfaces and higher dimensional objects, some important results regarding surfaces can not be extended to volumetric domains. Most significantly, there exist no conformal volumetric maps apart from Möbius transformations. Although it is sometime stated explicitly, it is often overlooked that existing methods of volume parameterization produce only quasi-conformal maps, which may be "far from conformality". We therefore introduce methods for assessing the extent of the local and global volumetric deformation by means of the amount of conformal distortion produced. To this end we first illustrate basic three-dimensional quasi-conformal deformations that are produced by parameterization techniques, and highlight theoretical issues associated with spatial quasi-conformal mappings, and the relation that exists between the geometry of the domain and conformal distortion.

1   INTRODUCTION

A conformal mapping, $f : \mathbb{R}^n \to \mathbb{R}^n$, is a 1:1 function that preserves angles between intersecting curves. Conformal maps are desirable in digital geometry processing and computer graphics, since they do not exhibit shear and, therefore preserve different vertex properties as well as the qualities of the mesh itself.

From a mathematical viewpoint, conformal mapping of a domain $D \subset \mathbb{R}^n$ is a smooth bijective function, which at any point $x \in D$ equally scales the space in every direction. This can be stated formally as

$$\forall h \in \mathbb{R}^n : \|df_x \cdot h\| = \|df_x\| \cdot \|h\|, \qquad (1)$$

where df_x denotes Jacobian matrix at point x.

The geometrical interpretation of (1) is that f transforms an infinitely small sphere to a sphere.

There is a wide range of applications in computer science and engineering for conformal parameterization and deformation of a surface. However, by a classical theorem of Liouville every conformal mapping of a domain in $\mathbb{R}^n, n \geq 3$, is restricted to be a Möbius transformation, i.e. a composition of translations, uniform scaling, linear isometry and inversion

in a sphere. Therefore, most of the real-world application can not produce conformal transformations of volumetric data. Instead the transformation yields the so called "quasi-conformal" mappings, which are close, in some sense to satisfying conformality. Such mappings can be understood intuitively as functions that approximately preserve angles.

One of the methods in computer graphics used to assess the degree of conformality of a 2D map f, is to consider the ratio of singular values in the domain D (Ahlfors, 2006),

$$\max_{x \in D} \frac{|\sigma_1(x)|}{|\sigma_n(x)|}, \qquad (2)$$

where $\sigma_1(x)$ and $\sigma_n(x)$ are the maximal and minimal singular values of df_x, respectively.

However, this approach is not accurate for dimensions greater than 2, since it examines the behaviour of f only in two directions.

In this paper we examine the problem of measuring the conformal distortion, produced by a 3D transformation. We also address issues related to the relation between the geometry of the volume and the minimal possible conformal distortion. Our approach is based on the theory of quasi-conformal homeomor-

(a) $\int_S H^2 dA = 3265$
$\int_S H dA = 25.25$

(b) $\int_S H^2 dA = 3124$
$\int_S H dA = 25.21$

(c) $\int_S H^2 dA = 2267$
$\int_S H dA = 28.2$
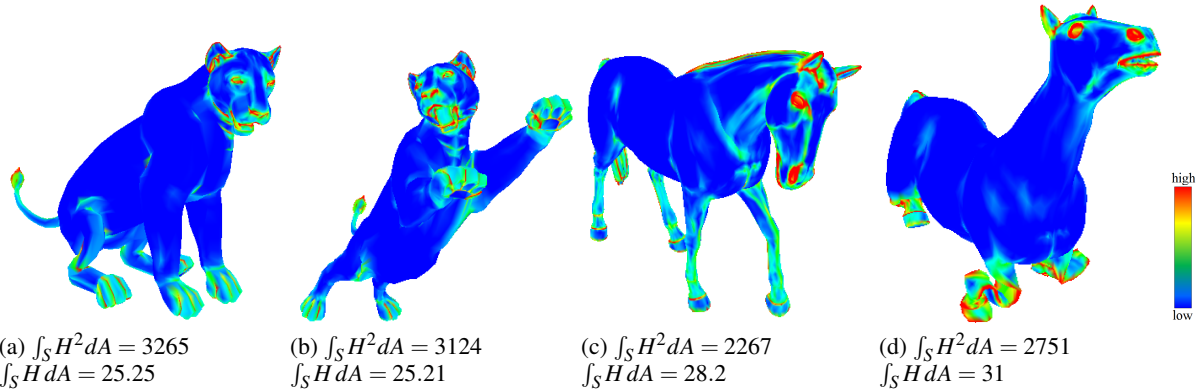
(d) $\int_S H^2 dA = 2751$
$\int_S H dA = 31$

Figure 1: Diagram of mean curvature distribution for deformations of polygonal models.
Figures 1(a),1(b) represent domain and image of nearly isometric deformation that decreases $\mathcal{W}$ and $\int_S H$ by 4.3% and 0.1%, respectively. Figures 1(c),1(d) represent domain and image of *qc*-deformation that increases $\mathcal{W}$ and $\int_S H$ by 21% and 10%, respectively.

phism in $\mathbb{R}^n$. More precisely, we shall examine the behaviour of f in a small neighbourhoods.

1.1 Conformal and isometric invariants

Given two homeomorphic domains D and D' in $\mathbb{R}^3$, we wish to measure how close are these domains to being conformally or isometrically equivalent. As the first step in this estimation, we focus on boundaries of the domains. We recall the following invariants of a closed surface:

- Willmore energy of a surface $S \subset \mathbb{R}^3$, which is conformal invariant (Willmore, 1993), defined by

$$\mathcal{W} = \int_S H^2 dA - 4\pi + 4\pi g(S), \qquad (3)$$

where H represents the mean curvature and $g(S)$ is the genus of a surface. For a practical results we assume that there are no changes in the genus. Thus, we shall compute conformal invariant as $\int_S H^2 dA$.

- Isometric invariant of a closed surface (Almgren and Rivin, 1999) is $\int_S H dA$.

Computation of invariants are shown in Figure 1 for triangular meshes, deformed by nearly-isometric and quasi-conformal transformations, obtained by discrete integration performed over the mesh vertices. The area element dA was approximated by area of barycentric cell around a vertex, mean curvature of a vertex was computed via the half-tube formula (Lev et al., 2007).

This method provides a naive approach for analysis of 3D domains, since it estimates only conformal distortion produced on the boundary of volumetric objects. To examine interior volumes we shall introduce the basic theory of quasi-conformal mappings

in $\mathbb{R}^n$. Based on this theory we shall review the relation between the conformal distortion and the surface of domains in subsection 3.6.

2 QUASI-CONFORMAL MAPS

2.1 Quasi-conformal dilatations

Quasi-conformal mappings in $\mathbb{R}^n$ can be studied by at least two alternative approaches. The first approach considers topological properties of a function along the integrable curves. The other approach, which we shall employ, examines the properties of a map in infinitely small neighbourhoods, where small spheres are transformed into ellipsoids.

First we are going to restrict ourself to linear transformations, for which we can define the following quantities.

Definition 1. *Let $A : \mathbb{R}^n \to \mathbb{R}^n$ be linear 1:1 transformation. Define*

$$K_I(A) = \frac{|\det A|}{l(A)^n}, \ K_O(A) = \frac{\|A\|^n}{|\det A|}, \qquad (4)$$

where

$$\|A\| = \max_{\|h\|=1} \|A \cdot h\|, \ l(A) = \min_{\|h\|=1} \|A \cdot h\|, \qquad (5)$$

and $K_I(A), K_O(A)$ are called inner and outer dilatations, respectively.

In the sequel we shall assume that all the functions $f : D \to D'$ are *diffeomorphisms*, that is f is a smooth bijective mapping with a smooth inverse. Hence, df_x is a full rank matrix, that maps a unit sphere $\mathbb{S}^n$ onto

<p align="center">(a) Original   (b) Cone, $\beta/\alpha = 1.4$ (c) Folding, $\beta/\alpha = 1.4$ (d) Radial, $a = 1.7$</p>
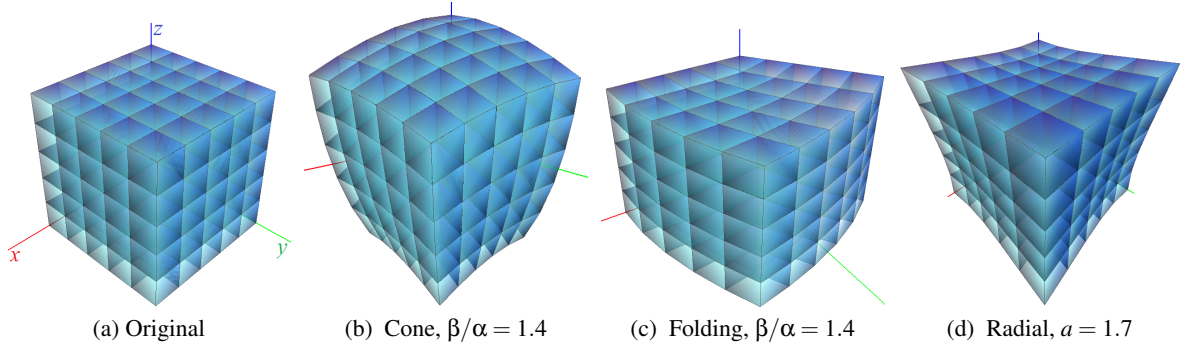
Figure 2: Basic quasi-conformal mappings of a $5 \times 5 \times 5$ grid.

an ellipsoid $E = df_x(\mathbb{S}^n)$. This leads itself to the following theorem:

Theorem 1. *Let $a_1 \geq a_2 \geq ....a_n$ be semi axes of E, then $a_1^2, ..., a_n^2$ are the eigenvalues of the matrix $df_x(df_x)^*$ and*

$$K_I(df_x) = \frac{a_1 \cdots a_{n-1}}{a_n^{n-1}}, \; K_O(df_x) = \frac{a_1^{n-1}}{a_2 \cdots a_n}. \quad (6)$$

Theorem 1 implies that $a_1, ..., a_n$ are the singular values of df_x. In particular, $a_1 = \|df_x\|$ is the longest of the semi-axes of the ellipsoid, while $a_n = l(df_x)$ is the shortest.

We define a *quasi-conformal dilatation* of f at a point x as

$$K(x) = \max\{K_I(df_x), K_O(df_x)\}, \quad (7)$$

and the *maximal quasi-conformal dilatation* of f as

$$K(f) = \max_{x \in D} K(x). \quad (8)$$

We call f *K-quasi-conformal*, denoted by *K-qc*, if $K(f) \leq K$ for some constant number K.

The value of $K(f)$ can be considered as a measure of departure from conformality of f. In particular, $K(f) \geq 1$, and the equality holds if and only if f is conformal.

2.2 Representation of volumetric data

Our first goal is to represent efficiently volumetric data, and to demonstrate interesting *qc*-deformations. We'll then compute, numerically, changes in geometrical properties of transformed domains. For these tasks we shall employ simple volumetric meshes, more precisely tetrahedal, and voxel meshes.

In addition to tetrahedral meshes produced from triangular models of closed surfaces by "Tetgen" library (Si, 2009), we introduce voxel meshes. Voxel meshes or voxelized volumes are regular hexahedral

meshes. Due to the regularity, voxel meshes are more stable for numerical computations, although they are much less flexible geometrically and generally represent only interior part of the volume.

Figure 4 depicts considerable differences in regularity and accuracy by which voxel and tetrahedral meshes represent the same volume. As can be observed, these differences become more pronounced after a series of *qc*-deformations.

We propose an algorithm for generating a voxel mesh from a polygonal mesh of a closed surface. Our Algorithm 1 of Voxelization procedure is similar to that of (Karabassi et al., 1999), with additional options for subdivision. This enables better approximations of continues domains with relatively low number of voxels. We run procedure Voxelize$(P, B, n_x, n_y, n_z, d, k)$ to generate voxel mesh M from polygonal mesh P of a closed surface, where B equals to the bounding box of P. The resulting mesh is denoted by

$$\text{voxel}(n_x, n_y, n_z; d; k). \quad (9)$$

We often use such values of n_x, n_y, n_z, that produce cubic voxels. In such cases we denote the resulting voxel-mesh by

$$\text{cubic}(n; d; k), \quad (10)$$

where n is the number of voxels along the longest axis of the bounding box B. Figure 3 shows cross sections of the torus, represented by various volumetric meshes, including both types of voxel meshes.

Testing whether a given point p is in interior of the mesh P, denoted int(P), was done by traversing ray from p and examining the number of intersection points between the ray and the mesh. A point p is an interior point of P if the number of intersection points is even. For efficient and stable intersection test we used ray traversing algorithm (Amanatides and Woo, 1987) and octree partition of the space (Perreault, 2007). Numerical issues may arise when a ray hits a

Algorithm 1: Voxelize(P,B,n_x,n_y,n_z,d,k)

Input:

P,B - polygonal mesh and bounding box

n_x,n_y,n_z - number of voxels along the axes.

d - max depth of subdivisions

k - number of voxels in subdivision

$M \leftarrow \varnothing$
if $d < 0$ **then**
$\quad$ Quit
Devide B into $n_x \times n_y \times n_z$ grid
foreach *voxel ϑ in the grid* **do**
$\quad$ **if** *All vertices of ϑ are inside P* **then**
$\quad\quad$ Add ϑ to M
$\quad$ **else if** *At least one vertex of ϑ is inside P*
$\quad$ **then**
$\quad\quad$ $B_\vartheta \leftarrow$ Bounding box of ϑ
$\quad\quad$ Voxelize($P,B_\vartheta, k,k,k, d-1, k$)

Output:

Partition of $B \cap \mathrm{int}(P)$ into voxel mesh M

(a) cubic(10;0;2)

(b) cubic(10;1;2)

(c) cubic(10;2;2)

(d) cubic(10;1;4)

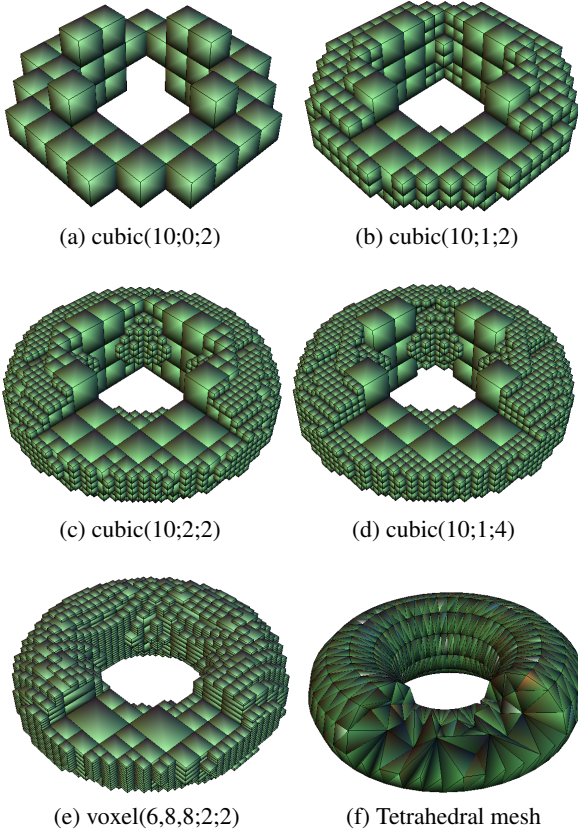(e) voxel(6,8,8;2;2)

(f) Tetrahedral mesh

Figure 3: Voxel meshes and the corresponding tetrahedral mesh. All meshes were generated from the same polygonal model of the torus.

vertex of P. To cope with these issues, we assume that two intersection points are equivalent if the distance between them is below some predefined threshold.

2.3 Examples of 3D quasi-conformal mappings

The simplest *K-qc*-map is an affine transformation. The linear part of the transformation determines *qc*-dilatation according to equation (4).

It's easy to construct simple *qc*-maps by linear transformations of cylindrical and spherical coordinates. Setting constant ratio $\beta/\alpha \geq 1$ we can construct a *folding* map in cylindrical coordinates by

$$F : (r,\varphi,z) \mapsto \left(r, \frac{\beta}{\alpha}\varphi, z\right), \ \varphi \in \left(0, \frac{2\pi\alpha}{\beta}\right), \quad (11)$$

and *cone* map in spherical coordinates by

$$C(r,\varphi,\theta) \mapsto \left(r, \varphi, \theta\frac{\beta}{\alpha}\right), \ \theta \in \left(0, \frac{\pi\alpha}{\beta}\right). \quad (12)$$

Computation of the *dF* yields (Väisälä, 1971, pp. 49–50)

$$K_I(F) = \beta/\alpha, \ K_O(F) = (\beta/\alpha)^2, \quad (13)$$

Let ρ be an inversion in the unit sphere $\mathbb{S}^3$, which is non-linear conformal map of $\mathbb{R}^3\backslash\{\mathbf{0}\}$. It's easy to extend ρ to a family of quasi-conformal maps ρ_a for $a \neq 0$ by

$$\rho_a(x) = \|x\|^{a-1}x \ \text{ for } x \neq \mathbf{0} \quad (14)$$

In particular $\rho = \rho_{-1}$ (see Fig. 4).

Computation of $d(\rho_a)_x$ shows that dilations of radial maps are domain-independent (Väisälä, 1971, p. 49):

$$K(\rho_a) = \begin{cases} \max\left\{|a|,a^2\right\} & |a| \geq 1 \\ \max\left\{a^{-2},|a|^{-1}\right\} & |a| \leq 1 \end{cases}. \quad (15)$$

We can construct more complicated *qc*-mappings by looking for an analogue of conformal functions in the plane. Zorich (Rickman, 1993) gave the example of mapping $Z : \mathbb{R}^3 \to \mathbb{R}^3\backslash\{0\}$, which can be seen as 3D extension of the complex exponential function. We shall present below *qc*-versions of the Zorich mapping:

Set $l > 0$ and define infinite cylinders:

$$\begin{aligned} C_l &= \left\{(x,y,z) \,|\, |x| \leq l, \, |y| \leq l\right\}, \quad (16) \\ \tilde{C}_l &= \left\{(x,y,z) \,|\, x^2 + y^2 \leq l^2\right\}, \end{aligned}$$
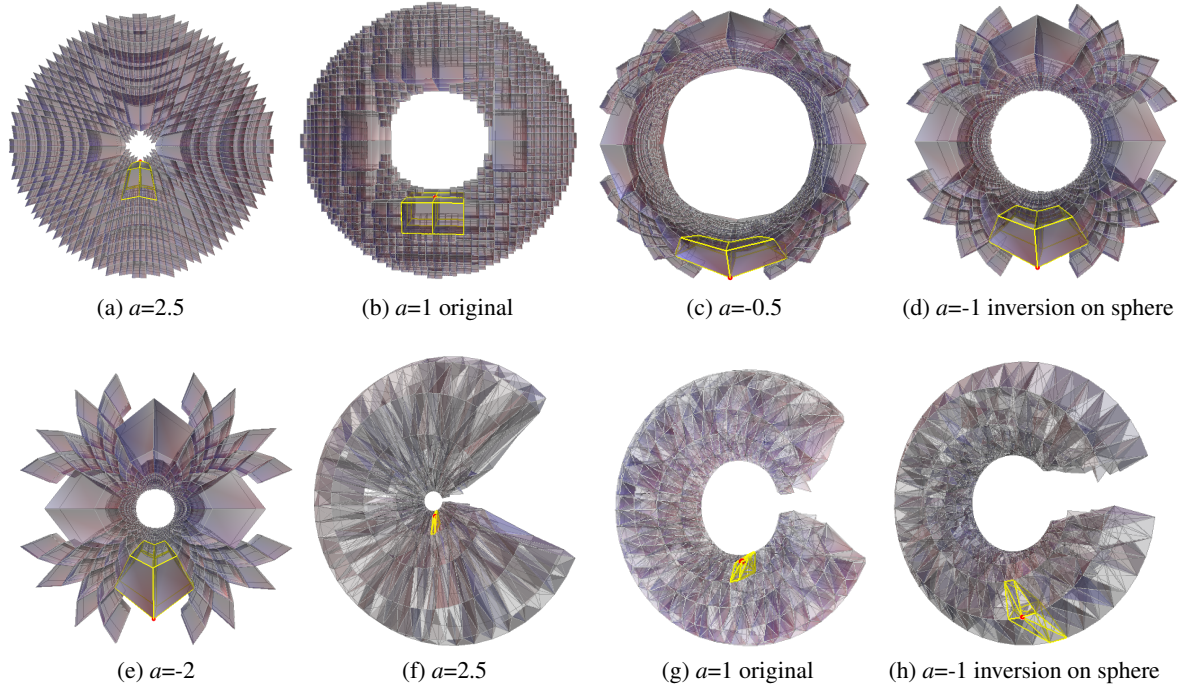
and consider the following functions:

Figure 4: Radial mappings of torus volume with different values of the parameter *a*. The torus is placed around origin and *y* axis. Figures 4(a)-4(e) represent the volume by voxel mesh of the type cubic(10;2;2). Figures 4(f)-4(h) show cross sections of the volume represented by tetrahedral mesh. Objects were rendered with transparency. Selected boundary vertex with its 1-ring were highlighted (relative sizes were not preserved).

i. A radial stretching in planes $\mathbb{R}^3 \times \{z\}$ of the square with edge $2l$ into the circle of radius l

$$Z_1 : \text{int}C_l \to \text{int}\tilde{C}_l \,.$$

ii. Quasi-conformal map of round cylinder into the half-space

$$Z_2 : \text{int}\tilde{C}_l \to \mathbb{H}\,,$$

defined by

$$Z_2 : (r, \varphi, z) \mapsto \left(e^{z/l}, \varphi, \frac{\pi r}{2l} \right), \quad (17)$$

where cylindrical and spherical coordinates, respectively, are used.

We define *Zorich* map as

$$Z : \text{int}C_l \to \mathbb{H}, \, Z = Z_2 \circ Z_1 \,. \quad (18)$$

This function can be applied on a model contained in C_l, thus we place models around the origin and set $l = a \cdot r$, where r is the radius of the bounding cylinder and $a \geq 1$ is a parameter that controls the distortion level.

Figure 2 illustrates basic *qc*-deformations of the cubic grid and Figure 5 shows some *qc*-mappings of the polygonal model.

2.4 Quasi-conformal parameterization

Consider a problem of volume parameterization into the unit ball $\mathbb{B}^3$. We shall restrict ourself to the following domains:

Definition 2. *Suppose D is a compact domain of $\mathbb{R}^3$ containing a point p. Denote by $\overline{px}$ the line segment connecting p and x. The domain D is called star-shaped at p, and p is called center of D if for any $x \in D$ $\overline{px} \subset D$.*

In particular, any convex domain is a star-shaped domain, where any interior point can serve as the center.

Without loss of generality, we shall focus on star-shaped domains at 0 that satisfy the following geometrical condition: for any $\zeta \in \partial D$, the angle between $\overline{\zeta 0}$ and tangent plane at ζ is larger than or equal to some constant $\alpha > 0$. Any point $x \neq \mathbf{0}$ of such domain D has a unique representation

$$x = u(x)\zeta(x)\,, \quad (19)$$

where $\zeta(x)$ is an intersection point of ∂D and $\overline{0x}$, and $u(x) = \|\zeta(x)\| / \|x\|$. Moreover, Caraman (Caraman, 1974, p. 408) had shown that for any $a > 0$ those do-

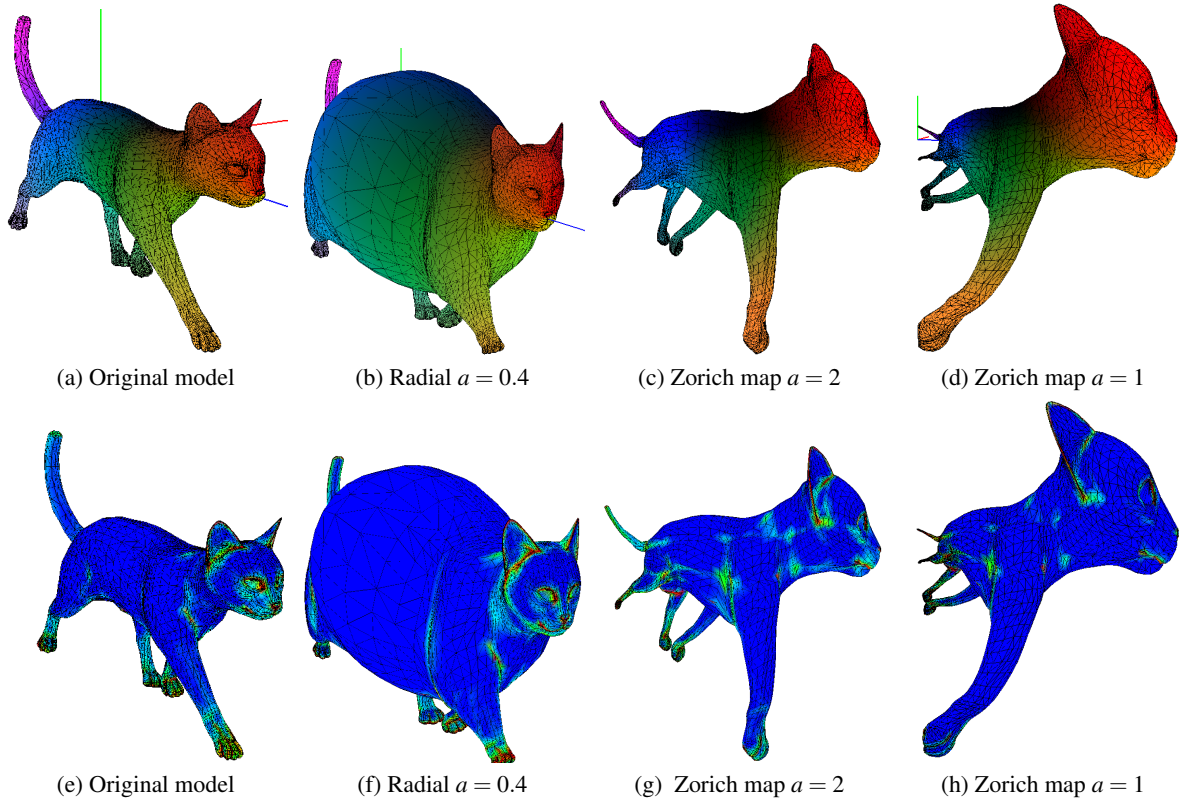|			
(a) Original model	(b) Radial $a = 0.4$	(c) Zorich map $a = 2$	(d) Zorich map $a = 1$
(e) Original model	(f) Radial $a = 0.4$	(g) Zorich map $a = 2$	(h) Zorich map $a = 1$

Figure 5: Quasi-conformal transformations of the polygonal mesh. 5(a)-5(d) are diagrams of spherical coordinates that visualize transformations by domain coloring technique. R,G,B color values in these figures correspond to r, φ, θ coordinates of the domain. 5(e)-5(h) are diagrams of mean curvature. Unit vectors are shown along the axes.

mains can be mapped quasi-conformally into $\mathbb{B}^3$ by

$$f(x) = \begin{cases} u(x)^a \dfrac{\zeta(x)}{\|\zeta(x)\|} & x \neq 0 \\ 0 & x = 0 \end{cases}. \qquad (20)$$

In fact any compact domain U, not necessarily star-shaped, that satisfies the geometrical condition can be mapped quasi-conformally by (20) into sub-domain of $\mathbb{B}^3$. We can consider U as a subdomain of a star-shaped domain D and redefine $\zeta(x)$ as the farthest point from $\mathbf{0}$ of the set $\partial D \cap \overline{\mathbf{0}x}$.

Figure 8 show this qc-parameterization of tetrahedral mesh into the unit ball for $a = 1$.

3 COMPUTATION OF QUASI-CONFORMAL DILATATIONS

Our aim is to compute numerically qc-dilatations of maps $f : D \to D'$ of discrete volumetric data, given the following input:

i. Two polyhedral meshes of the domain $M = (V, E, F, C)$ and of its image $M' = (V', E', F', C')$, where V, E, F and C are the vertex, edge, face and cell sets of M, respectively, with the same notion for M'.

ii. A transformation f defined on the set of mesh's vertices V. Depending on the context, we may use f as the correspondence function between the meshes.

$$f : (V, E, F, C) \to (V', E', F', C').$$

The initial data can be defined explicitly by a continuous domain D and by a procedure that computes $f(x)$ for any $x \in D$. In this case we have a freedom to generate appropriate polyhedral meshes to represent the data.

The only necessary assumption about f is that it should be a 1:1 function inside each polyhedral cell $c \in C$. To find qc-dilatation of f at vertex v placed at a position $x \in \mathbb{R}^3$, we need an estimation of the Jacobian matrix df_x, more precisely we approximate the following quantities: $\det(df_x)$, $\|df_x\|$ and $l(df_x)$.

Table 1: Weights of the cell in Ring(v).

i	$w_i(c)$	Description
1	1	Arithmetic average
2	$\mathrm{m}(c)$	Cell contribution is relative to its volume
3	$\Omega(c,v)$	Solid angle of c measured from the position of v
4	$\dfrac{\Omega(c,v)}{\mathrm{m}(c)}$	Combination of solid angle and reverse volume weights

3.1 Estimation of Jacobian determinant

It is well known from elementary calculus that for a diffeomorphism $f : D \to D'$

$$\int_{D'} dx' = \int_D J_f(x)dx, \; J_f(x) = \frac{dx'}{dx}, \quad (21)$$

where $J_f(x) = \det(df_x)$ will be referred as to "the Jacobian". Therefore an average value of the Jacobian inside a cell $c \in C$ can be approximated by the volume ratio

$$J_f(c) = \frac{\mathrm{m}(c')}{\mathrm{m}(c)}, \quad (22)$$

where $\mathrm{m}(\cdot)$ stands for a volume. We define a vertex Jacobian, denoted by $J_f(v)$, as the weighted average of the Jacobians in the neighboring cells

$$J_f(v) = \left(\sum_{c \in \mathrm{Ring}(v)} w(c) \frac{\mathrm{m}(c')}{\mathrm{m}(c)} \right) \left(\sum_{c \in \mathrm{Ring}(v)} w(c) \right)^{-1}, \quad (23)$$

where $\mathrm{Ring}(v)$ are the neighbouring cells of v and $w(c)$ is a chosen positive weight of the cell c (see Table 1) .

The volume of a tetrahedron τ with the vertex positions x_0, x_1, x_2, x_3 is

$$\mathrm{m}(\tau) = \frac{1}{6} \det\left(x_{10}, x_{20}, x_{30}\right), \quad (24)$$

where $x_{ij} = x_i - x_j$.

For a hexahedron c with the vertex positions $x_0, ..., x_7$ according to Figure 6(b) we can derive from (Dukowicz, 1988) the following formula :

$$\mathrm{m}(c) = \frac{1}{6} x_{70} \cdot \left(x_{10} \times x_{35} + x_{40} \times x_{56} + x_{20} \times x_{63}\right). \quad (25)$$

3.2 Weights for cells in 1-ring

Suppose we have a cell's property $P(c)$. We can estimate the corresponding property on a vertex $P(v)$ by a weighted average of $P(c)$, taken over the neighbouring cells $c \in \mathrm{Ring}(v)$. Table 1 summarizes some

methods to compute cell weights. In addition to the common methods such as arithmetic and volume averaging, we used the *solid angle* weights $\Omega(c,v)$ that measure which part of the ε-ball around v is occupied by c.

In a voxel mesh, each cell around a vertex v forms the same solid angle, therefore solid angle weights for voxels are equivalent to the arithmetic average.

Suppose τ is a tetrahedral cell shearing a vertex v and σ is the face of τ against v. In geometry $\Omega(\tau,v)$ is a measure of how large τ appears to an observer looking from v. Therefore $\Omega(\tau,v) = \Omega(\sigma,v)$, where the last quantity can be computed from (van Oosterom A, 1983).

3.3 Basic estimation of singular values

For a given vertex v and its edge e the length ratio $|e'|/|e|$ approximates $\|df_x \cdot h\|$ for a unit vector h in a direction of edge e. Thus according to (5), our estimations for the relevant singular values are

$$\|df_v\| = \max_{e \in \mathrm{Edge}(v)} \frac{|e'|}{|e|}, \; l(df_v) = \min_{e \in \mathrm{Edge}(v)} \frac{|e'|}{|e|}, \quad (26)$$

where $\mathrm{Edge}(v)$ is the set of the neighbouring edges of v.

The accuracy of this method depends on the *valence* of v, i.e. the number of edges connected to v, which is not always sufficiently large for a good approximation, especially for tetrahedal meshes, where irregular direction of edges could cause significant noise. (See Fig. 7(i) and 7(j).)

3.4 Estimation of Jacobian matrix

We can estimate qc-dilatation of f at vertex v, placed at a position $x \in \mathbb{R}^3$, based on estimation of the Jacobian matrix df_x. First we estimate the average matrix of df inside a given cell c, denoted by df_c. Then we define the vertex Jacobi matrix df_v as an average over df_c in the neighbouring cells.

Let $f^{(1)}, f^{(2)}, f^{(3)}$ be the coordinate components of the map f, where each one is a function from V to $\mathbb{R}$. We can express df_c as the matrix whose rows are the average gradient vectors of $f^{(i)}$.

Suppose r is a point inside tetrahedral cell τ, which consists of vertices v_1, v_2, v_3, v_4. Let σ_j be a face against v_j. Let s_j be the vector along the normal of σ_j, such that $\|s_j\| = \mathrm{Area}(\sigma_j)$ (see Fig. 6(a)), then for the piecewise linear extension of f we have by (Wang et al., 2003)

$$f^{(i)}(r) = \frac{1}{3\mathrm{m}(\tau)} \sum_{j=1}^{4} (r \cdot s_j) f^{(i)}(v_j). \quad (27)$$
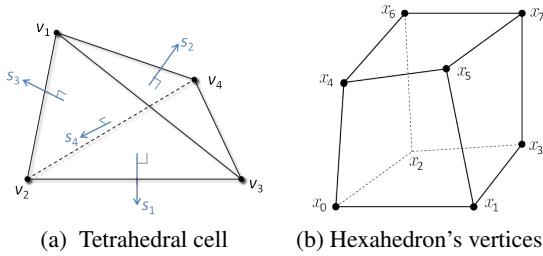
(a) Tetrahedral cell (b) Hexahedron's vertices

Figure 6: Cells of volumetric mesh.

(a) 0.1 (b) 0.01 (c) 0.0005
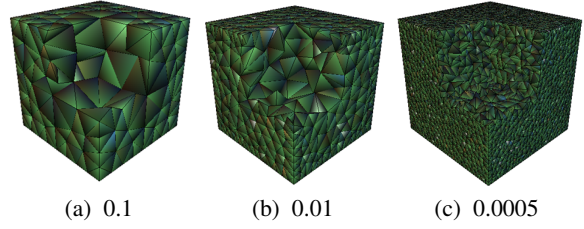
Figure 9: Cross sections of tetrahedral meshes of the unit cube. The maximal cell volume is indicated below each figure.

This implies that the gradient is constant inside τ, hence our estimates give

$$\nabla f^{(i)}(\tau) = \frac{1}{3\mathrm{m}(\tau)} \sum_{j=1}^{4} s_j f^{(i)}(v_j); \qquad (28)$$

and

$$\nabla f^{(i)}(v) = \sum_{c \in \mathrm{Ring}(v)} \nabla f^{(i)}(c) \omega(c), \qquad (29)$$

where $\omega(c)$ are normalized weights from the table 1

$$\omega(c) = \frac{w(c)}{\sum\limits_{\eta \in \mathrm{Ring}(v)} w(\eta)}. \qquad (30)$$

We can extend above formulas for hexahedral mesh without triangulation in a following way.

Suppose hexahedron c consists of vertices $v_1, ..., v_8$, and faces $\sigma_1, ..., \sigma_6$ (the enumeration is arbitrary). Similarly to tetrahedron case, we define s_j to be a vector along the normal of σ_j such that $\|s_j\| = \mathrm{Area}(\sigma_j)$. Denote by $\bar{\sigma}_j$ the face against σ_j. The face $\bar{\sigma}_j$ contains 4 vertices against the face σ_j, we shall substitute them by single dummy vertex u_j placed at the center of $\bar{\sigma}_j$. The value of $f(u_j)$ can be approximated by an average over the face $\bar{\sigma}_j$

$$f(u_j) \approx \frac{1}{4} \sum_{v \in \bar{\sigma}_j} f(v). \qquad (31)$$

Combining all the above for each component of f, we have

$$\nabla f^{(i)}(c) = \frac{1}{4\mathrm{m}(c)} \sum_{j=1}^{6} \left(\sum_{v \in \bar{\sigma}_j} f^{(i)}(v) \right) s_j. \qquad (32)$$

In a similar way this formula can be extended to an arbitrary polyhedral cell.

For a voxel cell ϑ, with dimensions $\alpha \times \beta \times \gamma$, centered at point p, (32) yields the following estimation:

$$\nabla f_\vartheta^{(i)} = \frac{1}{4\alpha\beta\gamma} \sum_{v \in \vartheta} f^{(i)}(v) \cdot (s_1\beta\gamma, s_2\alpha\gamma, s_3\alpha\beta), \qquad (33)$$

where s_k is the sign of the kth component of $v - p$.

The matrix df_v, derived from the gradients vectors yields an approximation of a continuous Jacobian matrix df_x, then it is straightforward to estimate the vertex Jacobian via

$$J_f(v) = \det \left(\nabla f^{(1)}(v), \nabla f^{(2)}(v), \nabla f^{(3)}(v) \right). \qquad (34)$$

Moreover, the singular values $a_1 = \|df_v\|$ and $a_3 = l(df_v)$ can be approximated as the maximum and minumum of $\|df_v \cdot h_j\|$ sampled at random directions $h_1, \ldots, h_m$.

3.5 Results and validation

We present results of numerical computations of qc-dilatation for various domains and maps. We employ the following default methods of computations, unless stated otherwise. Singular values are computed from the estimation of Jacobian matrices, described in subsection 3.4, while Jacobians are approximated by a volume ratio (22). Solid angle weights were used for tetrahedral meshes, and arithmetic average for voxel meshes.

Figure 7 summarizes results for the Zorich mapping with $a = 1$ of the unit sphere, represented by both voxel and tetrahedral meshes. One can notice the correlation between areas on the surface of higher values of qc-dilations and areas of higher values of mean curvature and dihedral angles. From comparison of figures 7(e),7(f) with the figures 7(i),7(j), it is obvious that gradient methods for singular values are preferable over the methods of length ratios.

Figure 8 depicts no visible correlation between qc-dilatations and Jacobian values, shown for parameterization of the tetrahedral model.

To validate our approach we selected qc-mappings with known dilatations and compared our numerical results with the theoretical values. The simplest qc-mappings were examined first. Estimations for a linear map showed the exact theoretical value for $\max K$ of the domain with the precision of 10^{-5}. The same accuracy was achieved for Jacobian and singular values at the chosen point. Folding map, which is a linear
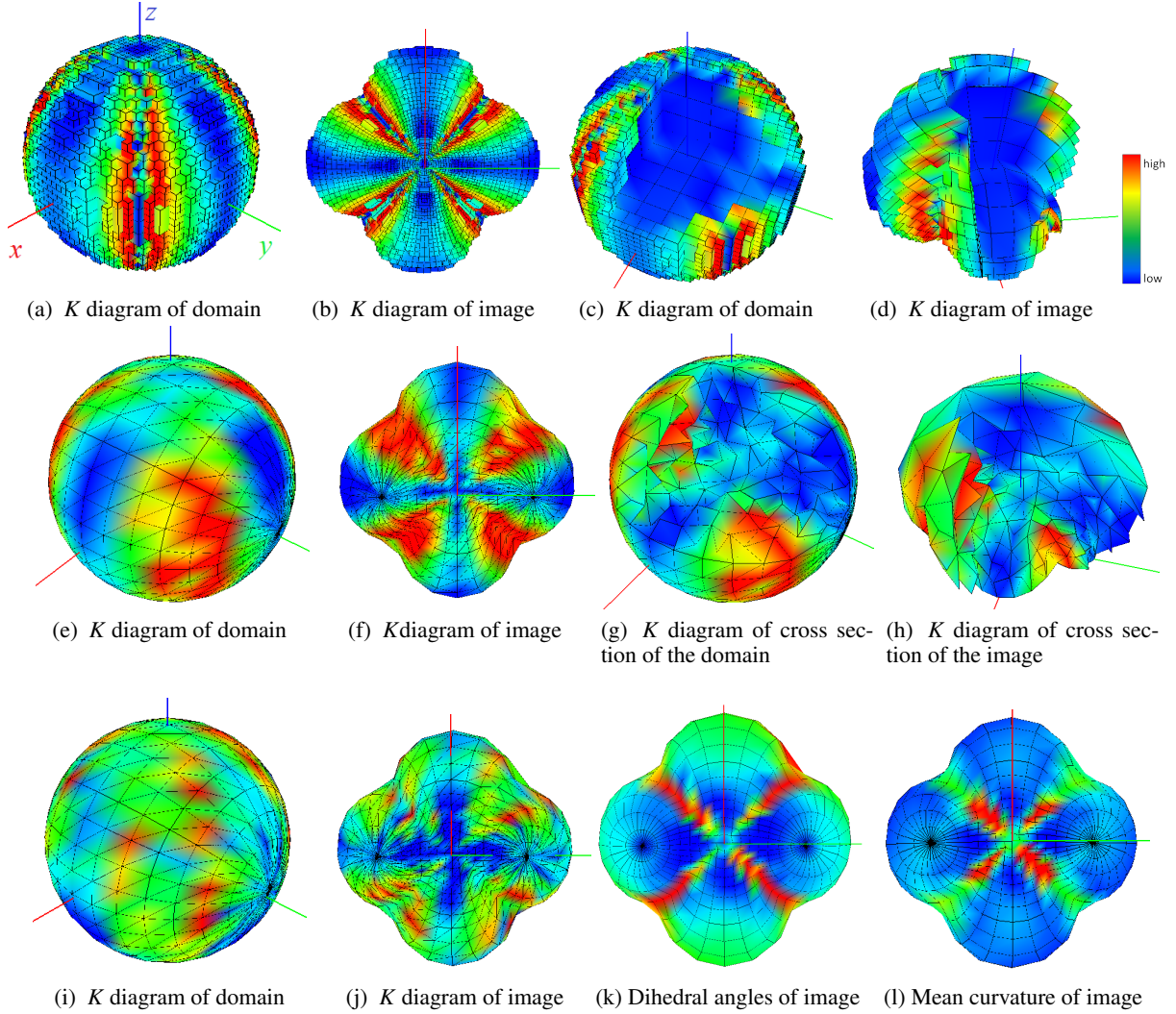
(a) *K* diagram of domain (b) *K* diagram of image (c) *K* diagram of domain (d) *K* diagram of image

(e) *K* diagram of domain (f) *K* diagram of image (g) *K* diagram of cross section of the domain (h) *K* diagram of cross section of the image

(i) *K* diagram of domain (j) *K* diagram of image (k) Dihedral angles of image (l) Mean curvature of image

Figure 7: Zorich mapping with $a = 1$ of the ball placed at the origin. Dilatations were computed by default method except 7(i) and 7(j), where the singular values were estimated by the length ratio method. Figures 7(a)-7(d) are voxel meshes, 7(e)-7(j) are tetrahedral meshes, and 7(k), 7(l) are triangular meshes of volumes' boundaries. Max K values, obtained for tetrahedral and voxel meshes, are 4.6 and 4.55, respectively.

map in cylindrical coordinates, also gave close results to the theory, according to the table 2.

Figure 10 shows the relations that exist between numerical estimation of maximal *qc*-dilatation K and maximal cell size of a mesh. These computations were performed for the same radial map on 2 domains represented by different volumetric meshes. As expected, numerical estimations of max K converges to the exact theoretical value as the maximal cell size approaches zero. This is basically due to the fact that our estimates are based on piecewise linear approximations of f, which converge to f when the maximal cell size goes to zero.

Table 2: Folding maps for different values of β/α were applied on tetrahedral and voxel meshes of the torus parallel to xz plane, placed at (0,2,0). Voxel mesh is denoted according to (10).

Mesh type	β/α	max K	Exact max K
cubic(10;2;2)	0.5	3.996	4
	1.5	2.249	2.25
	2	3.997	4
Tetrahedral	0.5	4.01	4
	1.5	2.264	2.25
	2	4.063	4

3.6 Quasi-conformal coefficients

While there is an abundance of conformal mappings in 2D, general volumetric domains can be mapped

(a) Domain

(b) Image

(c) Cross section of the domain

(d) Image of the cross section

(e) K diagram of domain

(f) K diagram of image

(g) K diagram of domain

(h) K diagram of image

(i) Jacobian diagram of domain

(j) Jacobian diagram of image

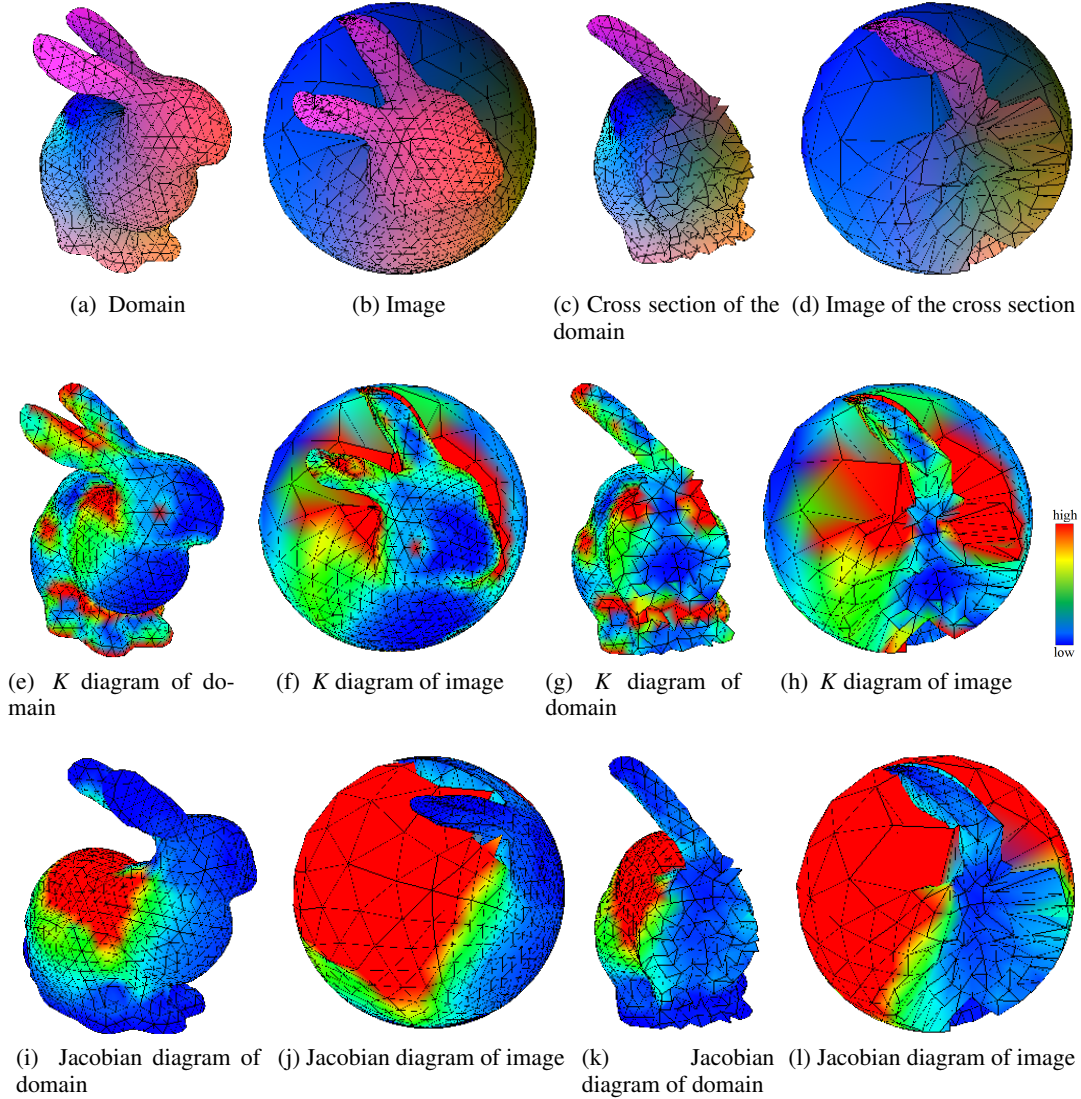(k) Jacobian diagram of domain

(l) Jacobian diagram of image

Figure 8: Radial stretching of the tetrahedal models from the center of the bounding box to the unit ball. The figures show diagrams of different vertex properties in the domain and in the image. Cross sections were obtained by crossing yz plane. Figures 8(a)-8(d) are diagrams of spherical coordinates with the same color coding as in Figure 5.

only quasi-conformally. Therefore one of the challenges in 3D is to measure the minimal conformal distortion required to map one domain into another. The corresponding quantity is called a *quasi-conformal coefficient* of domains D and D', and it is defined as

$$K(D,D') = \inf K(f), \qquad (35)$$

where the infimum is taken over all *qc*-mappings $f : D \to D'$. The problem to compute $K(D,D')$ for arbitrary domains, is generally unsolvable. Therefore we should focus on lower bounds and specific 3D domains. Our main interest will be *qc*-coefficient $K(D,\mathbb{B}^3)$, which corresponds to parameterizations of volumes into the unit ball.

Volumes are generated from polygonal models which, in fact, are surfaces of 3D polyhedrons. Intersections of adjacent faces of polyhedron forms 3D *wedges*, which can be mapped by a similarity transformation to

$$D_\alpha = \left\{ (r,\varphi,z) \in \mathbb{R}^3 \,\middle|\, 0 < \varphi < \alpha,\, r > 0 \right\}, \qquad (36)$$

defined in cylindrical coordinates for some angle α.

Let's define the following related notations.

Definition 3. *A domain W is called a wedge of angle α, If there exists a similarity transformation*
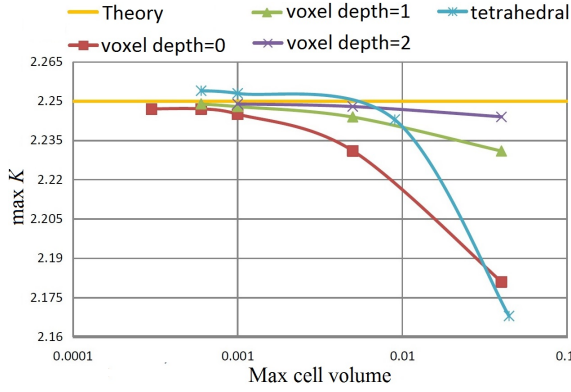
$$S : W \to D_\alpha.$$

Figure 10: Relation between max cell volume of volumetric meshes, shown on a logarithmic scale, and accuracy of the max K computation. Voxel meshes were generated from the torus surface with different depth values and a raising number of divisions (see Fig. 4). Tetrahedral meshes were generated from the surface of the unit cube with different restrictions on the quality and on the maximal cell volume (see Fig. 9). All the volumes were transformed by the radial map for $a = 1.5$, for which max $K = 2.25$, as given by equation (15).

Definition 4. *A point b of a domain D is called a wedge point of angle* α*, if* $b \in \partial D$ *and there exists neighbourhood U of b such that* $U \cap W = U \cap D$*, where W is a wedge of angle* α *.*

Suppose that qc-transformation f maps some wedge point of angle α to a wedge point of angle β, for $0 < \alpha \le \beta \le \pi$. Väisälä (Väisälä, 1971, pp. 132–135) had concluded that in a small neighbourhood of the wedge points, f behaves like a folding map defined in (11). This fact implies the following inequality

$$K_I(f) \ge \beta/\alpha. \qquad (37)$$

Inequality (37) shows that in contrast to the 2D case, there is no general conformal map between 3D wedge points.

Consider the half-space D_π. It can be mapped into a ball by inversion in the unit sphere placed at $(0, 0, -1)$. Since the composition with a conformal map preserves qc-dilatations (Väisälä, 1971, p. 43), we have

$$K(D, \mathbb{B}^3) = K(D, D_\pi) \qquad (38)$$

and, if D has a wedge point of angle α, by (37)

$$K(D, \mathbb{B}^3) \ge \pi/\alpha. \qquad (39)$$

According to (Caraman, 1974, p. 434), the maximal dihedral angle of a convex polyhedron P with m faces is

$$\frac{(m-3)\pi}{m-1}. \qquad (40)$$

This, along with (39), yields the simple estimation

$$K(P, \mathbb{B}^3) \ge \frac{m-1}{m-3}. \qquad (41)$$

Moreover, (37) implies that the minimal possible qc-dilatation of the mapping between tetrahedral meshes $f : M \to M'$ is the maximal ratio of dihedral angles

$$\max \frac{\measuredangle((f(\sigma_i), f(\sigma_j))}{\measuredangle(\sigma_i, \sigma_j)}, \qquad (42)$$

taken over adjacent faces σ_i, σ_j of the surface of M. In particular, for a parameterization onto a cube

$$K(f) \ge \max \frac{\pi/2}{\measuredangle(\sigma_i, \sigma_j)}, \qquad (43)$$

and for a parameterization onto a ball, we have

$$K(f) \ge \max \frac{\pi}{\measuredangle(\sigma_i, \sigma_j)}, \qquad (44)$$

since the half-plane and a ball are conformally equivalent.

Figure 11 shows a series of convex polyhedrons with raising number of faces. Each polyhedron was mapped to $\mathbb{B}^3$ by a radial stretching described in (20). The resulting values of maximal dilatations K are consistent with (41). As one can assert from the figure, maximal values of K are obtained at boundary vertices. These boundary vertices are the wedge points that prescribe the lower bound for K_I.

4 CONCLUSIONS

Deformations and parameterizations of discrete volumes are employed in such areas of engineering and science as Solid Modeling, MRI data processing etc. Our quantitative method of computing qc-dilatations provides a natural metric for estimation of the global and local quality of volume deformation. This method is readily available for comparison with other techniques that are used in volumetric parameterizations, e.g. discrete harmonic energy (Wang et al., 2003).

Among other applications, our approach can be used to produce desirable deformations and parameterizations of 3D domains, by minimizing the maximal qc-dilatation under the given conditions.

The problem of parameterization of star-shaped domains was studied by (Xia et al., 2010). We presented a simple technique for quasi-conformal parameterization of volumes into the unit ball. This technique is based on radial stretching of star-shaped domains. It can be extended to more general domains, such as a set of connected convex segments.
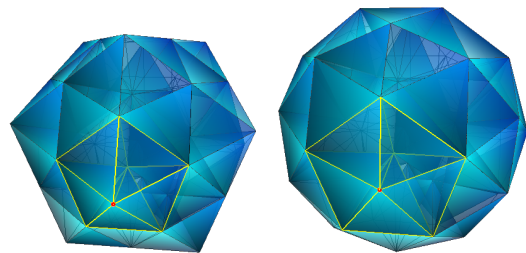
According to the obtained numerical results and theoretical propositions, qc-dilatations are tightly related to distortion of such geometrical properties as
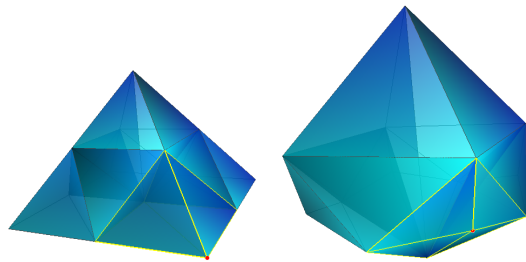
(a) 5 faces, max $K = 12$, average $K = 4.7$
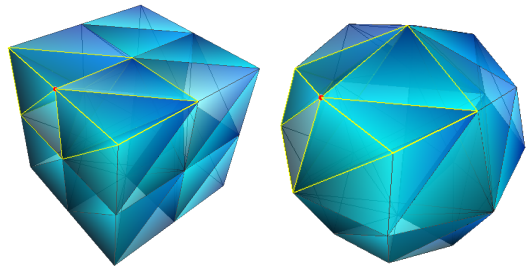
(b) 6 faces, max $K = 4.5$, average $K = 3.6$

(c) 20 faces, max $K = 1.8$, average $K = 1.5$

Figure 11: Parameterization of convex polyhedrons, performed by the radial stretching toward the unit ball, with $a = 1$. Each figure shows, from left to right, tetrahedral mesh of domain and image. Highlighted areas are the 1-rings of the vertices that reached maximal dilatation. Keep in mind, that parameterization is applied on vertices and it does not refine meshes. Therefore the surface of the resulting image can deviate from being round.

mean curvature and dihedral angles. Additional mathematical research is currently in progress with the goal in mind of further theoretical interpretation of this and related result.

ACKNOWLEDGEMENTS

REFERENCES

Ahlfors, L. V. (2006). *Lectures on quasiconformal mappings.* Providence, RI: American Mathematical Society (AMS), 2nd enlarged and revised edition.

Almgren, F. J. and Rivin, I. (1999). The mean curvature integral is invariant under bending. In *The David Epstein 60th birthday Festschrift*. International Press.

Amanatides, J. and Woo, A. (1987). A fast voxel traversal algorithm for ray tracing. In *Eurographics '87*, pages 3–10. Elsevier Science Publishers, Amsterdam, North-Holland.

Caraman, P. (1974). *n-dimensional quasiconformal (QCF) mappings. Revised, enlarged and translated from the Roumanian by the author.*

Dukowicz, J. (1988). Efficient volume computation for three-dimensional hexahedral cells. *Journal of Computational Physics.*

Karabassi, E.-A., Papaioannou, G., and Theoharis, T. (1999). A fast depth-buffer-based voxelization algorithm. *Journal of Graphics Tools: JGT*, 4(4):5–10.

Lev, R., Saucan, E., and Elber, G. (2007). Curvature estimation over smooth polygonal meshes using the half tube formula. In Martin, R. R., Sabin, M. A., and Winkler, J. R., editors, *IMA Conference on the Mathematics of Surfaces*, volume 4647 of *Lecture Notes in Computer Science*, pages 275–289. Springer.

Perreault, S. (2007). *Octree C++ Class Template.* http://nomis80.org/code/octree.html.

Rickman, S. (1993). *Quasiregular mappings*, chapter 1, page 15. Berlin: Springer-Verlag.

Si, H. (2009). *A Quality Tetrahedral Mesh Generator and Three-Dimensional Delaunay Triangulator.* Tetgen, http://tetgen.berlios.de.

Väisälä, J. (1971). *Lectures on n-Dimensional Quasiconformal Mappings.* Springer-Verlag Berlin Heidelberg New York.

van Oosterom A, S. J. (1983). The solid angle of a plane triangle. In *IEEE Trans Biomed Eng.*

Wang, Y., Gu, X., Yau, S.-T., et al. (2003). Volumetric harmonic map. In *Communications in Information & Systems*, volume 3, pages 191–202. International Press of Boston.

Willmore, T. (1993). *Riemannian geometry.* Oxford: Clarendon Press.

Xia, J., He, Y., Han, S., Fu, C.-W., Luo, F., and Gu, X. (2010). Parameterization of star-shaped volumes using green's functions. In Mourrain, B., Schaefer, S., and Xu, G., editors, *GMP*, volume 6130 of *Lecture Notes in Computer Science*, pages 219–235. Springer.